Axial Diffusion of Liquids in Packed Beds and End Effects

A. W. LILES and C. J. GEANKOPLIS

The Ohio State University, Columbus, Ohio

Experimental data were obtained on the effect of bed length of packed spheres on axial diffusion coefficients with the frequency response technique used. Lengths of packed section of 6 to 174 cm. were used. The end effects were eliminated by using a novel experimental technique for analyses of the inlet and outlet streams. No effects of length on D_L were found.

When the end effects were artificially introduced by using void analytical sections at the two ends, then large effects of length on D_L were found. These void sections were the cause of length effects found by other experimenters. The D_L drops as the length of bed is increased. Above about 65 cm. length the D_L remains constant with increase in length. The over-all results are in general agreement with the data of others.

An understanding of the behavior of fluids in empty tubes and packed beds is very important in the study of heat, mass, and momentum transfer. Much experimental data exist on radial mass transfer or diffusion coefficients perpendicular to the axial flow of the liquid or gas. Recently Ebach and White (*3*), Carberry and Bretton (*1*), and Strang and Geankoplis (*7*) presented experimental correlations for packed beds of spheres for the effect of liquid velocity, particle diameter, and viscosity on the axial diffusion coefficient.

However no comprehensive experimental study has been made of the elimination of end effects and the effect of column length on D_L for liquids. McHenry and Wilhelm (*5*) obtained data on gases for different lengths and eliminated end effects by calculation. Carberry and Bretton (*1*) presented experimental points obtained at five different bed lengths and different velocities using liquids.

To investigate the axial diffusion of a flowing system experimentally the outlet response resulting from an inlet disturbance is measured. This disturbance can be a step or pulse function or a continuous sine-wave function. The sine wave is used in the frequency response experiments. Ebach and White (*3*) discuss these methods in detail.

In the present work D_L values were obtained for glass spheres in packed beds with water used. End effects were experimentally eliminated which removed the column length effect on D_L. The effect of length was also determined by introducing end effects artificially and varying the length.

THEORY

All equations discussed below are derived for a packed bed of nonporous solids, continuous flow, and a sine-wave input. The basic theory for the frequence response method has been derived by Rosen and Winsche (*6*) and modified by others (*1, 2, 3, 5, 7*). All derivations start with the following partial differential equation:

$$D_L \frac{\partial^2 C}{\partial Z^2} - U \frac{\partial C}{\partial Z} = \frac{\partial C}{\partial t} \qquad (1)$$

It is assumed that C is a function of Z and t only, that there are no radial gradients, and that U is constant. Carberry and Bretton (*1*) discuss in detail the assumptions implied in this model. Their data and that of others (*3*) suggest that Equation (1) does not apply owing to the fact the amplitude does not dampen as the square root of time or bed length. However in the present work it will be shown that it does apply under the carefully designed conditions of experimentation.

Two boundary conditions are imposed at the inlet and the outlet of the bed respectively:

$$C_{(0,\,t)} = C_M + A_{(0)} \sin \omega t \qquad (2)$$

$$C_{(\infty,\,t)} = C_M \text{ or } A_{(Z)} = 0 \text{ for } Z \to \infty \qquad (3)$$

When one uses the above three equations, the final integrated equation can be obtained by the Laplace transform and details of the derivations are given elsewhere (*4*). The periodic steady state solution is

$$C_{(L,\,t)} = C_M + A_{(0)} e^{-B} \sin(\omega t - \xi) \qquad (4)$$

where B is

$$B = \frac{UL}{2D_L}\left\{ \sqrt[4]{1 + \left(\frac{4\omega D_L}{U^2}\right)^2} \cdot \cos\left[\frac{\tan^{-1}\left(\frac{4\omega D_L}{U^2}\right)}{2} \right] \left\{ -1 \right\} \right. \qquad (5)$$

Ebach and White (*3*) get

$$B = \frac{-UL}{2D_L}\left\{ 1 - \sqrt{\sqrt{\frac{1}{4} + \left(\frac{2D_L\omega}{U^2}\right)^2} + \frac{1}{2}} \right\} \qquad (6)$$

When one expands the radicals and trigonometric functions in series and drops the higher-order terms, Equations (5) and (6) both yield the same equation:

$$B = \frac{L\omega^2 D_L}{U^3} - \frac{5L\omega^2 D_L^3}{U^7} \qquad (7)$$

If the last term is negligible

$$B = \frac{L\omega^2 D_L}{U^3} \qquad (8)$$

The equation for the phase shift referred to the bed entrance is

$$\xi_{\text{Calc.}} = \frac{UL}{2D_L}\sqrt{\sqrt{\frac{1}{4} + \left(\frac{2D_L\omega}{U^2}\right)^2} - \frac{1}{2}} \qquad (9)$$

After one expands and drops higher-order terms, the equation reduces to

$$\xi_{\text{Calc.}} = \frac{\omega L}{U} \qquad (10)$$

This can be compared to the phase shift measured experimentally. Deisler and Wilhelm (*2*) discuss in detail the addition of $n\pi$ radians to the $\xi_{\text{Exp.}}$. Equation (9) could be used to compare D_L obtained from phase shift to that determined by amplitude change in Equation (7) at short column lengths.

If a column has three different sections of packing in series where the first section (0, 1) and the third section (2, 3) have identical packing and the middle section packing (1, 2) is

A. W. Liles is with Esso Standard Oil Company, Baton Rouge, Louisiana.

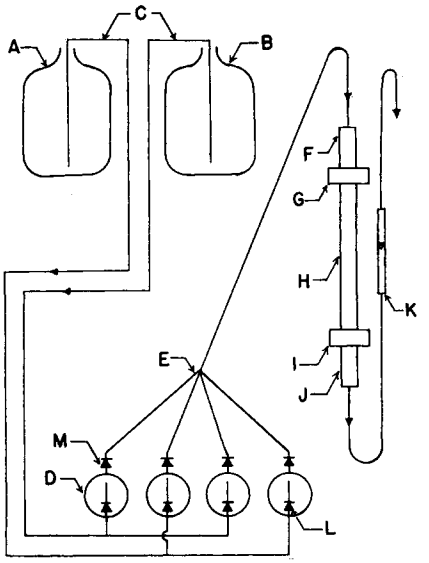

Fig. 1. Process flow diagram.

different, then an equation can be derived as follows:

$$B_{0,1} = \ln \frac{A_0}{A_1},\ B_{2,3} = \ln \frac{A_2}{A_3},\ B_{1,2} = \ln \frac{A_1}{A_2} \tag{11}$$

Now if $L_{0,1} = L_{2,3}$ and $U_{0,1} = U_{2,3}$, then $D_{L_{2,3}} = D_{L_{0,1}}$ since the conditions in both sections are identical. By Equation (7) $B_{0,1} = B_{2,3}$. The quantity $B_{0,3}$ is measured experimentally, and

$$B_{0,3} = \ln \frac{A_0}{A_3} = \ln \frac{A_0}{A_1} + \ln \frac{A_1}{A_2} + \ln \frac{A_2}{A_3} \tag{12}$$

Rearranging one gets

$$\ln \frac{A_1}{A_2} = B_{1,2} = B_{0,3} - [B_{0,1} + B_{2,3}] \tag{13}$$

Equation (13) can be shown to be identical with the result of McHenry and Wilhelm (5) which was derived in a different way.

EXPERIMENTAL METHODS

Apparatus

The apparatus (Figure 1) is a modification of that used by Strang and Geankoplis (7). The items are (A) 2-naphthol solution storage bottle, (B) water storage bottle, (C) pump suction lines, (D) four, single-action positive-displacement pumps, (E) discharge and mixing manifold, (L) and (M) ball check valves, (F) packed inlet section to remove higher harmonics, (G) upper analytical section, (H) packed test section, (I) lower analytical section, (J) packed outlet section, (K) outlet rotameter.

A variable-drive cam-operated apparatus actuates the four pumps, and one revolution results in two sine-wave periods. For some high-velocity runs or to vary the frequency and keep the bed velocity constant water was added by means of a gear pump at the inlet to (F) or solution was withdrawn at this point (Figure 1).

Analytical

Figure 2 shows the novel analytical section made of aluminum and held in the external flange (B). The flat silica windows (D) were held against the analytical section housing by a brass plate (C) and a gasket (F). The analytical grating (E) was composed of three ¼ in. sq. brass rods. The two ⅛ in. open slits were formed to allow solution and light to pass through. The void area open to liquid flow was approximately that of the packed section of 6-mm. glass beads which were stacked around and could not enter the slits (Figure 2). No screens were used in this section. This analytical section simulates a packed bed. The concentration of the tracer 2-naphthol in the solution affects the amount of light passing through the slits and going to the phototubes. Details are given elsewhere (4).

A strip-chart recorder was used to record the output of the phototubes (4). The recorder was calibrated twice each day at the beginning and end of a series of runs by passing known solutions through the tower. The maximum concentration of 2-naphthol was 10 ppm. During a run inlet concentration waves were first recorded and then outlet waves (Figure 3). The curves are very close to a true sine wave.

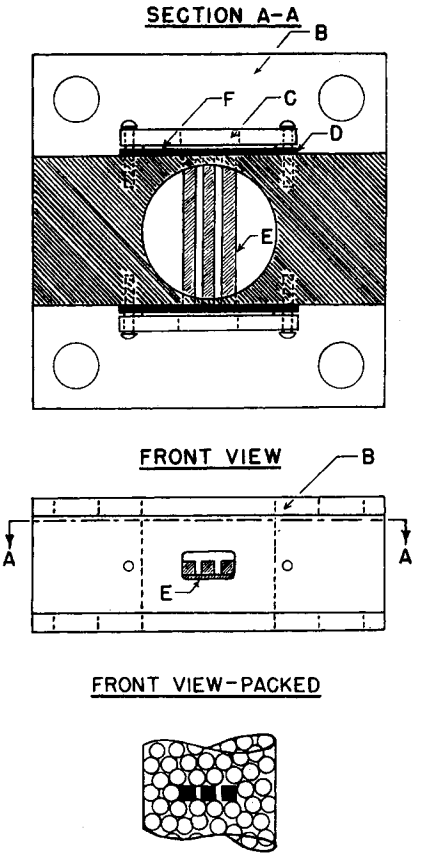

Fig. 2. Details of analytical section.

Distilled water and Coleman and Bell CP 2-naphthol were used. The diameter of the spherical glass beads used and the average void volumes were 6.13 mm. (0.40), 3.21 mm. (0.39), and 0.47 mm. (0.36).

EXPERIMENTAL DATA AND CALCULATIONS

Typical experimental data are given in Table 1, detailed data are given elsewhere (4). The data were obtained at an average temperature of 77°F. Column length, velocity, frequency,

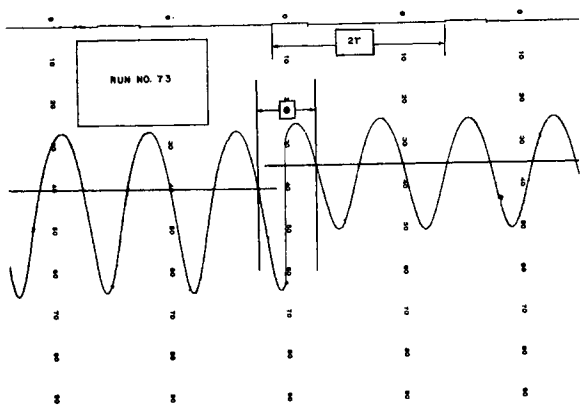

Fig. 3. Instrument trace of inlet and outlet waves.

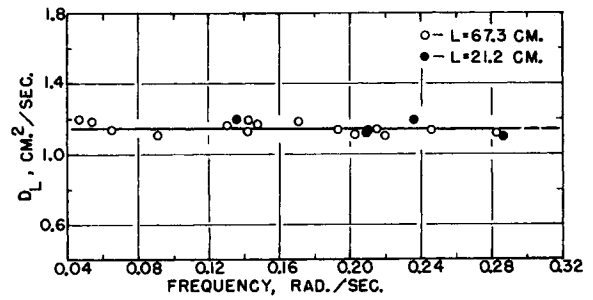

Fig. 4. Effect of frequency on D_L (data corrected to U = 1.20 cm./sec.).

TABLE 1. TYPICAL EXPERIMENTAL RUNS

Run no.	L, cm.	U, cm./sec.	D_L, sq.cm./sec.	N_{Re}	N'_{Re}	N_{Ps}	ξ Calc.	ξ Exp.
			6.13-mn. Glass beads					
133	5.85	1.44	1.33	105	41.5	0.67	0.67	0.66
81	21.2	0.61	0.64	36.9	15.1	0.59	2.52	2.58
18	36.4	0.87	0.91	65.0	25.6	0.59	4.21	4.21
123	67.3	3.67	3.14	266	105	0.72	6.10	6.25
94	98	2.71	2.35	207	81.8	0.71	11.4	11.3
49	128	2.60	2.14	187	75.6	0.74	15.7	15.7
67	174	2.82	2.44	187	76.5	0.71	21.4	20.9
			3.21-mm. glass beads					
169	67.3	1.44	0.65	49.6	19.3	0.71	7.60	7.66
173	67.3	3.21	1.45	111	43.3	0.71	7.50	7.41
			0.47-mm. glass beads					
178	61.2	1.29	0.164	6.54	2.37	0.370	7.12	7.05
183	61.2	2.60	0.344	13.0	4.70	0.355	6.99	7.03
			6.13-mm. glass beads (open or void analytical section)					
140	18.4	1.38	3.17	105	43.0	0.267	2.74	2.81
153	64.5	1.44	1.56	109	43.0	0.57	8.15	8.06
148	171	1.60	1.50	125	48.8	0.65	20.7	20.7

and diameter of packing were varied. Also in twenty-nine of the runs a completely open or void analytical section was used instead of the slits to find out if the void sections caused end effects.

In Figure 3 the distance between two timing pips combined with the chart speed represents 2τ. The quantity θ was determined by measuring the distance between the intersection of the 50% concentration point of inlet and outlet waves. With knowledge of the chart speed θ and the frequency, $\xi_{Exp.}$ was obtained. In some cases $n\pi$ radians were added to obtain the correct $\xi_{Exp.}$ (2). The column length L used was the packed distance between analytical slits.

The $\xi_{Calc.}$ was obtained by means of the simplified Equation (10) or the exact Equation (9) when the error with the simplified equation exceeded 3%. In the runs with open analytical sections the $\xi_{Calc.}$ was equal to the sum of the phase angle calculated for the packed bed plus that of the open sections.

To calculate D_L Equation (7) was generally used. When the calculation error exceeded 3%, the exact Equations (5) or (6) were utilized. In runs with the 0.47-mm. packing, this packing was used in the test section and 6.13-mm. packing used in the section above the inlet slits and below the outlet slits. This was necessary, since the slits would otherwise become filled with packing. Equation (13) was used to calculate $B_{1,2}$ and then Equations (5), (6), or (7) for D_L.

DISCUSSION

Frequency, Phase Angle, and Length Effects

To find the effect of frequency, data at a constant velocity of 1.20 cm./sec. were obtained. As expected, Figure 4 shows no effect of frequency on D_L with an average deviation from the line of ±2.8%. This is within the accuracy of the experimental data.

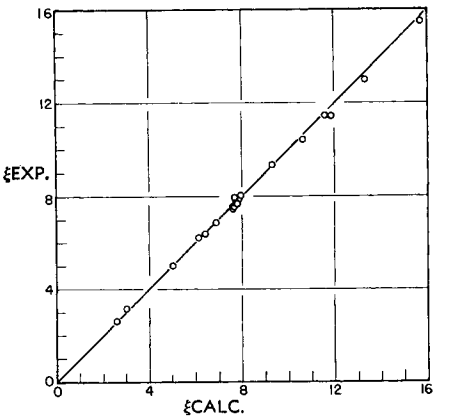

Fig. 5. Comparison of phase angles (L = 67.3 cm., d_p = 6.13 mm.).

McHenry and Wilhelm (5) state that the calculated and experimental phase angles should check each other. Equation (10) shows that for long bed lengths the calculated phase angle is merely the calculated mean residence time multiplied by the measured frequency. In Figure 5 the measured and calculated phase angles check within an average deviation of ±1.6% for L = 67.3 cm. which shows merely that the mean residence time and frequency were accurately measured. Similar results were obtained for other long lengths and also when analytical slits were used. However for short lengths Equation (10) gave results which were off by up to 15% when compared with the experimental results. Use of Equation (9) reduced the errors to less than 3% which gives a partial check on D_L obtained by amplitude change and phase shift.

In Figure 6 D_L is plotted vs. U for packed lengths varying from 5.85 to 174 cm. The average deviation from the line is less than ±3% for 6.13-mm. packing. This shows conclusively that there is no effect of length for the large 6.13-mm. packing and that end

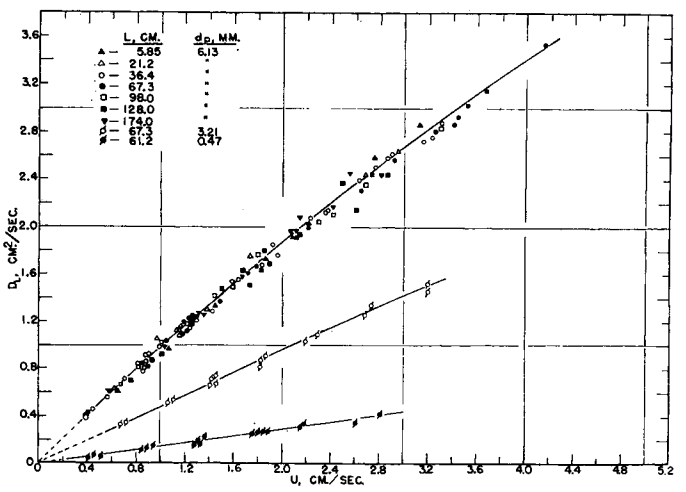

Fig. 6. Effect of velocity on D_L.

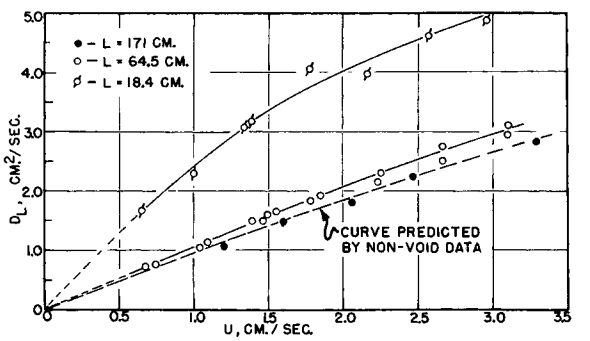

Fig. 7. Effect of void analytical sections on D_L (6.13-mm. spheres).

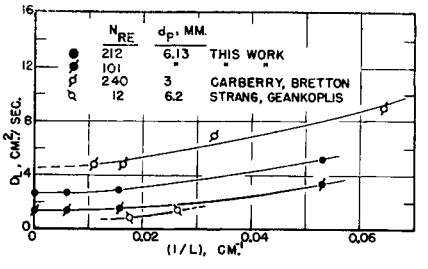

Fig. 8. D_L as an inverse function of L (for void analytical sections).

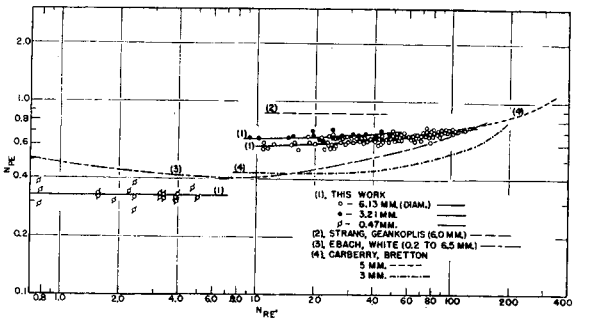

Fig. 9. Comparison of data with that of other investigators for beds greater than 59 cm. long, Peclet number as function of Reynolds number for spheres.

effects have been eliminated experimentally by using the novel analytical slits with the same void fraction as the packing. This also shows that the data obey Equation (1). This amplitude-length behavior indicates the absence of appreciable capacitance effects. Since only one bed length was investigated for the smaller particle sizes, it was not possible to prove or disprove the effect of length or the presence of capacitance effects for smaller particles as found by others (*1*). Strang and Geankoplis (*7*) found a similar trend of D_L vs. velocity for one column length. McHenry and Wilhelm (*5*) using gases eliminated end effects by an indirect method using experimental correction factors.

Effect of Velocity

Data with no end effects and all column lengths were plotted for the three sizes of spheres on a log-log scale with all lines having the same slopes. The data can be represented as follows for the 6.13, 3.21, and 0.47-mm. spheres respectively:

$$D_L = 0.958U^{0.98} \qquad (14)$$

$$D_L = 0.498U^{0.98} \qquad (15)$$

$$D_L = 0.148U^{0.98} \qquad (16)$$

When one combines Equations (14), (15), and (16)

$$D_L = 1.25\,(d_p)^{0.73}U^{0.98} \qquad (17)$$

This effect of diameter is inconclusive, since only three different sizes were used. Ebach and White (*3*) found that for 6.76- and 3.48-mm. beads the exponent of U was 1.08 in low-velocity regions less than 2 cm./sec. and decreased markedly at higher velocities. For very small spheres they found an exponent of 1.08 up to high velocities. Bed lengths used were 61 cm. and longer. It appears that the exponent may vary somewhat over a wide velocity range.

A similar plot with the data with the end effects (open or void analytical sections) shows that data for the 171- and 64.5-cm. lengths yield a slope of 0.93 also. The data for the 18.4-cm. length show a slope of 0.76.

Effect of Void Analytical Sections

The data obtained by the use of void analytical sections of 2.78 cm. in length had packed sections of different lengths. The void or open sections were similar to those used by Strang and Geankoplis (*7*), McHenry and Wilhelm (*5*), Ebach and White (*3*), and Carberry and Bretton (*1*). Their lengths of open section varied from about ½ to 1¼ in. The data of this work are plotted in Figure 7 and the shortest packed length gives the greatest D_L values. The present work has now shown experimentally that the bed entrance and exit effects caused by the void sections were the primary reasons for previously observed amplitude-bed length anomalies of other investigators (*1, 3, 7*). These were correctly explained theoretically by McHenry and Wilhelm (*5*).

At the long packed lengths the D_L values are the same as the data for the nonvoid sections. This is to be expected, since the end effects would be negligible at the infinite bed lengths. Similar phenomena were reported for liquid-liquid extraction towers (*8*).

In several runs the width of the analytical opening for analysis in the void section was varied from 3/16 to 1/2 in. with no differences noted.

The data for different packed column lengths having void analytical sections are also plotted in Figure 8. The data of this work were obtained from cross plots of Figure 7 and the points for infinite column length, that is no end effects, from Figure 6. The data of Carberry and Bretton (*1*) show the same trends as this work. For lengths over 171 cm. the end effects are negligible. The data of Strang and Geankoplis (*7*) for two column lengths show similar trends.

Correlation of Peclet Numbers

When one uses the data of this work with no end effects, the Peclet numbers for the 0.47-mm. spheres in Figure 9 are significantly lower than the values for the larger diameters. The line for the 3.21-mm. spheres is about 8% higher than that for the 6.13-mm. spheres. Ebach and White (*3*) state that at a given Reynolds number the same Peclet number is obtained for all diameters, but their data scatter quite widely. It appears that much work needs to be done on the effects of particle diameter.

Using only data for spheres with packed lengths over 57 cm. to eliminate most end effects a comparison can also be made with data available in the literature (Figure 9). Average lines were drawn through the data of each investigator. The maximum spread of the 3- and 5-mm. sphere data of Carberry and Bretton (*1*) from one average line through their data is ±20%, ±50% for Ebach and White (*3*), ±50% for Strang and Geankoplis (*7*), and ±12% for this work. Because of this large spread of the data there is general agreement of all investigators. More data are needed especially at high Reynolds numbers over 400 to determine if the Peclet number continues to rise as the Reynolds number is increased, which is indicated in Figure 9. The data of Carberry and Bretton (*1*) and this work indicate an increase in Peclet number with increasing sphere diameter. However the work of Ebach and White (*3*) show no trend with diameter. The 5-mm. sphere line of Carberry and Bretton (*1*) starting at a Reynold's number of 34 is almost identical with the 6.1-mm. sphere line of this work.

ACKNOWLEDGMENT

The authors express their appreciation to the General Electric Charitable and Educational Fund for support of graduate fellowships during the course of this work.

NOTATION

$A_{(0)}$ = amplitude of wave at Z = 0, g./ml.

$A_{(Z)}$ = amplitude of wave at Z = Z, g./ml.

B = ln (A_0/A_L)
C = concentration as a function of position Z and time t, g./ml.
$C_{(L,\ t)}$ = concentration at Z = L and $t = t$, g./ml.
C_M = mean concentration, g./ml.
$C_{(0,\ t)}$ = concentration at Z = 0, and $t = t$, g./ml.
$C_{(\infty,\ t)}$ = concentration at Z = ∞ and $t = t$, g./ml.
D_L = axial diffusion coefficient, sq. cm./sec.
d_p = diameter of particle, cm.
L = packed bed length, cm.
n = number 1, 2, 3, . . .
N_{Pe} = Peclet number = $d_p U/D_L$
N_{Re} = Reynolds number = $d_p U\rho/\mu$
N'_{Re} = Reynolds number = $d_p U'\rho/\mu$
t = time, sec.
U = interstitial velocity in bed, cm./sec.
U' = velocity based on empty tube, cm./sec.
Z = longitudinal distance in bed, cm.

Greek Letters

θ = distance between intersection of 50% points, cm.
τ = wave period, sec.
ξ = phase angle, radians
μ = viscosity, poise
ρ = density, g./ml.
ω = angular frequency, radians/sec.

LITERATURE CITED

1. Carberry, J. J., and R. H. Bretton, *A.I.Ch.E. Journal*, 4, 367 (1958).
2. Deisler, P. F., Jr., and R. H. Wilhelm, *Ind. Eng. Chem.*, 45, 1219 (1953).
3. Ebach, E. A., and R. R. White, *A.I.Ch.E. Journal*, 4, 161 (1958).
4. Liles, A. W., Ph.D. dissertation, Ohio State Univ., Columbus, Ohio (1959).
5. McHenry, K. W., Jr., and R. H. Wilhelm, *A.I.Ch.E. Journal*, 3, 83 (1957).
6. Rosen, J. B., and W. E. Winsche, *Chem. Phys.*, 18, 1587 (1950).
7. Strang, D. A., and C. J. Geankoplis, *Ind. Eng. Chem.*, 50, 1305 (1958).
8. Vogt, H. J., and C. J. Geankoplis, *ibid.*, 46, 1763 (1954).

Manuscript received October 19, 1959; revision received February 15, 1960; paper accepted February 18, 1960.

The Role of Porosity in Filtration: IV. Constant Pressure Filtration

F. M. TILLER and H. R. COOPER

University of Houston, Houston, Texas

Certain assumptions which have previously served as a basis for the conventional equations employed in constant pressure filtration are shown to be in error. It is demonstrated that the specific filtration resistance, the ratio of the mass of wet to mass of dry cake, and the rate of flow, $q = dv/d\theta$, are not constant as has been assumed. In an example it is shown that q undergoes an eightfold variation as the liquid flows from the cake surface through to the medium.

Since the product αq appears in the basic differential equation, incorrect values of q lead to errors in the calculated values of α arising from experimental data. The errors are significant when thick slurries are employed.

New partial differential equations are presented for flow through compressible media in which q varies with cake thickness. Modifications of the conventional constant pressure equations are presented.

In the conventional analysis of constant pressure cake filtration (*1, 3, 4*), three approximations are made which may be invalid under certain circumstances. In the Ruth filtration equation

$$q = \frac{dv}{d\theta} = \frac{1}{\mu}\,\frac{g_c\,p}{\left[\dfrac{\alpha s \rho}{1-ms}\,v + R_m\right]} \qquad (1)$$

It is generally assumed for constant pressure operation that the filtration resistance is constant, the ratio of the mass of wet to mass of dry cake is constant, and at any instant the rate of flow $dv/d\theta$ is constant throughout the cake. Analysis of basic phenomena indicates that these assumptions must be modified and that discrimination must be employed for correct use of Equation (1). The first two postulates are primarily in error in the initial period of filtration. Consequently it is in rotary filtration and in abbreviated experimental determinations of cake characteristics where the time of filtration is frequently short that the employment of constant values of α and m may lead to erroneous results. The assumption involving the constancy of $dv/d\theta$ may be strikingly in error for thick slurries.

H. R. Cooper is with The Fluor Corporation, Ltd., Los Angeles, California.

PRESSURE AT MEDIUM

In Figure 1 a filter cake is illustrated in which flow of fluid takes place from left to right, and distance is measured from the surface of the cake. As the liquid flows frictionally through the compressible, porous media, p_s drops until it reaches the value p_1 at the interface of the cake and supporting medium.

The pressure at the medium is defined by

$$g_c\,p_1 = \mu\,R_m\,q_1 = \mu\,R_m\,\frac{dv}{d\theta} \qquad (2)$$

where $q_1 = dv/d\theta$ is the rate of filtrate flow in (cubic feet)/(square feet)(second). The relationship of time to pressure p_1 at the medium and the pressure drop across the cake $(p - p_1)$ is illustrated in Figure 2 for talc filtered at a constant pressure of 5 lb./sq. in. Initially when there is no cake, the entire pressure drop is across the medium and $p = p_1$. As $dv/d\theta$ decreases with time, p_1 falls in accord with Equation (2) and the pressure drop $(p - p_1)$ across the cake builds up.

In general a medium should be chosen to give a minimum resistance consistent with the production of satisfactory clarity. Grace (2) has indicated that a filter medium exhibiting a resistance equivalent to no more than 0.01 in. of cake can usually be selected with the result that the pressure drop across the medium becomes a negligible portion of the total pressure drop for a major portion of the filter cycle.